JBC Papers in Press. Published on June 22, 2010 as Manuscript M109.099424
The latest version is at http://www.jbc.org/cgi/doi/10.1074/jbc.M109.099424

Deficiency of chemokine receptor CCR1 causes osteopenia due to impaired functions of osteoclasts and osteoblasts

Running title: Role of CCR1 in bone metabolism

Akiyoshi Hoshino[1,3,5], Tadahiro Iimura[4], Satoshi Ueha[2], Sanshiro Hanada[1], Yutaka Maruoka[1,6], Mitsuori Mayahara[7], Keiko Suzuki[8], Toshio Imai[9], Masako Ito[10], Yoshinobu Manome[5], Masato Yasuhara[3], Takaaki Kirino[11], Akira Yamaguchi[4], Kouji Matsushima[2], and Kenji Yamamoto[1,3]*

1 International Clinical Research Center, Research Institute, International Medical Center of Japan, Tokyo 162-8655, JAPAN; 2 Department of Molecular Preventive Medicine, Graduate School of Medicine, the University of Tokyo, Tokyo 113-0033, JAPAN; 3 Department of Pharmacokinetics and Pharmacodynamics (Hospital Pharmacy), and 4 Department of Oral Pathology, Global Center of Excellence, Tokyo Medical and Dental University, Tokyo 113-8519, JAPAN; 5 Department of Molecular Cell Biology, Institute of DNA Medicine, Research Center for Medical Sciences, Jikei University School of Medicine, Tokyo 105-8461, Japan; 6 Department of Dentistry and Oral Surgery, Toyama National Hospital, International Medical Center of Japan, Tokyo 162-8655, Japan; 7 Department of Oral Histology, and 8 Department of Pharmacology, Showa University School of Dentistry, Tokyo 142-8555, JAPAN; 9 Kan Research Institute, Inc., Kobe 650-0047, JAPAN;10 Department of Radiology, Nagasaki University School of Medicine, Nagasaki 852-8501, Japan; 11 President of International Medical Center of Japan, Tokyo 162-8655, JAPAN.

*Address corresponding to: Kenji Yamamoto (M.D, Ph.D.), International Clinical Research Center, Research Institute, International Medical Center of Japan. Toyama 1-21-1, Shinjuku-ku, Tokyo 162-8655, Japan. Tel.: +81-3-3202-7181 ext.2856 or 5611, e-mail: backen@ri.ncgm.go.jp

Chemokines are characterized by the homing activity of leukocytes to targeted inflammation sites. Recent research indicates that chemokines play more divergent roles in various phases of pathogenesis as well as immune reactions. The chemokine receptor, CCR1, and its ligands are thought to be involved in inflammatory bone destruction, but their physiological roles in the bone metabolism *in vivo* have not yet been elucidated. In the present study, we investigated the roles of CCR1 in bone metabolism using CCR1-deficient mice. *Ccr1*$^{-/-}$ mice have fewer and thinner trabecular bones and low mineral bone density in cancellous bones. The lack of CCR1 affects the differentiation and function of osteoblasts. *Runx2*, *Atf4*, *Osteopontin*, and *Osteonectin* were significantly upregulated in *Ccr1*$^{-/-}$ mice despite sustained expression of *Osterix* and reduced expression of *Osteocalcin*, suggesting a lower potential for differentiation into mature osteoblasts. In addition, mineralized nodule formation was markedly disrupted in cultured osteoblastic

cells isolated from *Ccr1*$^{-/-}$ mice. Osteoclastogenesis induced from cultured *Ccr1*$^{-/-}$ bone marrow cells yielded fewer and smaller osteoclasts due to the abrogated cell-fusion. *Ccr1*$^{-/-}$ osteoclasts exerted no osteolytic activity concomitant with reduced expressions of *Rank* and its downstream targets, implying that the defective osteoclastogenesis is involved in the bone phenotype in *Ccr1*$^{-/-}$ mice. The co-culture of wild-type osteoclast precursors with *Ccr1*$^{-/-}$ osteoblasts failed to facilitate osteoclastogenesis. This finding is most likely due to a reduction in *Rankl* expression. These observations suggest that the axis of CCR1 and its ligands are likely to be involved in crosstalk between osteoclasts and osteoblasts by modulating the RANK–RANKL-mediated interaction.

Chemokines are initially identified as small cytokines that direct the homing of circulating leukocytes into sites of inflammation (1). Chemokines are now recognized to be major factors in inflammation and immune development as well as tumor growth, angiogenesis, and osteolysis. Chemokine receptors are expressed in a well-organized spatio-temporal manner in various types of leukocytes, including lymphocytes, granulocytes, and macrophages. They facilitate the recruitment of these cells into inflammatory sites during the appropriate phase of inflammation.

Recent findings indicate that chemokine receptors including CCR1 and its related chemokines, CCL3 and CCL9, are involved in the pathogenesis of a variety of diseases. In particular, CCL3 (also called MIP-1α), a major proinflammatory chemokine produced at inflammatory sites, appears to play a crucial role in pathological osteoclastogenesis (2,3). In osteolytic bone inflammation (e.g., rheumatoid arthritis-associated bone destruction), CCL3 induces ectopic osteoclastogenesis (4) and results in bone destruction (5). Several reports suggested that CCL3 is also produced by myeloma cells, and directly stimulates bone destruction in myeloma-related bone diseases (5-7). These findings indicate the possible roles of CCL3 as a crucial chemokine for osteoclast function. Several antagonists of the chemokine ligands of CCL3, such as CCR1-specific (BX471) and CCR5-specific (TAK779) blockers, have been tested as drug candidates for the treatment of patients with rheumatoid arthritis-associated bone destruction and multiple myeloma (4,8). The chemokine CCL9 (also called MIP-1γ), is also abundantly produced by various myeloid lineage-derived cells, including osteoclasts (9), activates osteoclastogenesis through its receptor, CCR1 (10-12). However, the exact physiological functions of CCR1 and its related chemokines in bone remodeling are still not fully characterized (12,13).

A recent study using an ovariectomy-induced bone loss model found that the chemokine receptor CCR2 was associated with postmenopausal bone loss (14), but there are few reports on bone phenotypes in other chemokine receptor-deficient mouse models. In the present study, we demonstrated that osteopenia in *Ccr1*$^{-/-}$ mice appeared to be due to

impaired osteoclast and osteoblast function. Our data also uncovered a possible role for CCR1 and its related ligands in the communication between osteoclasts and osteoblasts.

Experimental procedures

Mice– Standard male C57BL/6 mice (6-9 weeks of age) were obtained from CLEA Japan. *Ccr1*$^{-/-}$ mice (15) purchased from Jackson Laboratories were backcrossed for 8 to 10 generations on the C57BL/6 background mice. Mice were all bred and maintained under pathogen-free conditions at the animal facilities of the University of Tokyo. All experiments were performed according to the Institutional Guidelines for the Care and Use of Laboratory Animals in Research and were approved by the ethics committees of both the University of Tokyo and the Research Institute of International Medical Center of Japan.

Materials– Recombinant mouse M-CSF and RANKL were purchased from R&D Systems Inc (Minneapolis, MN, USA) and PeproTech Inc (Rocky Hill, NJ, USA), respectively. Recombinant mouse CCL2 (MCP-1), CCL3 (MIP-1α), CCL4 (MIP-1β), CCL5 (RANTES), CCL9 (MIP-1γ) and CCL11 (eotaxin-1), and their corresponding neutralizing antibodies were purchased from R&D Systems. Control rat IgG was purchased from Jackson ImmunoResearch (Bar Harbor, ME, USA). Recombinant mouse CX3CL1 (fractalkine) was purchased from R&D Systems. Hamster anti-CX3CL1 neutralizing antibody and control hamster IgG were kindly provided by Dr. Toshio Imai (Kan Research Institute, Kobe, Japan). Rabbit anti-human/mouse CCR1 polyclonal antibody and control rabbit IgG were purchased from AbCam (Cambridge, MA, USA) and Chemicon (Temecula, CA, USA), respectively. Secondary antibodies (Alexa488-labeled anti-rabbit IgG and Streptavidin-PE) were purchased from Molecular Probes (Eugene, OR, USA). Rabbit anti-TRAP and anti-Cathepsin K polyclonal antibodies were both purchased from Santa Cruz Biotechnology (Santa Cruz, CA, USA).

Osteoclast and osteoblastic cell culture– Mouse bone marrow cells cultured in α-MEM were used as sources of osteoclastic and osteoblastic cell cultures. The non-adherent cells were collected for bone marrow-derived macrophage and pre-osteoclast induction, and adherent bone marrow-derived mesenchymal stromal cells were collected for osteoblast induction. Bone marrow-derived macrophages were induced with 10 ng/ml M-CSF for an additional 10 days. To generate pre-osteoclasts, non-adherent cells were passed through a column filled with Sephadex G-10 microspheres (Amersham biosciences), and were then cultured with 10 ng/ml M-CSF and 20 ng/ml RANKL for 4 days. The mature osteoclasts were induced from pre-osteoclasts by culturing for an additional 14 days with M-CSF and RANKL. The culture media were replaced every three days. TRAP activity in the osteoclasts was determined by staining using an acid phosphatase leukocyte staining kit (Sigma Chemical, Saint Louis, MO, USA). The contamination of stromal/osteoblastic cells was monitored using Q-PCR analysis, as a low expression level of the *Osteoprotegrin* gene

indicates stromal/osteoblastic cells.

Osteoblastic differentiation in adherent bone marrow mesenchymal stromal cells was induced by culture in α-MEM containing 10% FBS, 200 μM ascorbic acid, 10 mM β-glycerophosphate and 10 nM dexamethasone (16). The culture media was replaced once every three days in the presence or absence of chemokine neutralizing antibodies. The cells were fixed with 4% paraformaldehyde, and stained for alkaline phosphatase with naphthol AS-MX phosphate plus Fastblue-BB (Sigma) and for minerals with alizarin red. Mineral deposition was alternatively identified by von Kossa staining (Polysciences, Inc., Warrington, PA, USA), and the mineralized areas were measured by Array Scan VTI HCS analyzer (Beckman Coulter).

Co-culture experiments with osteoclast precursors and osteoblasts were performed by inoculating bone marrow-derived precursors (1×10^5 cells/well) onto the layer of osteoblastic cells that had been cultured for 21 days with osteoblast-inducing media in 24-well plates. Thereafter, these cells were co-cultured for 7 days in α-MEM supplemented with 10% FBS and 10 μg/ml vitamin D_3. To assess bone resorption activity, these co-culture studies were also conducted using bone slices. After fixation of the cells with 2.5% glutaraldehyde/1.6% paraformaldehyde in 0.1M cacodylic acid (pH 7.4), the bone slices were briefly rinsed, and were completely dehydrated in an ascending series of ethanol and liquid carbon dioxide. The samples were coated with an ultrafine titanium oxide powder, and were observed under scanning electron microscopy.

Immunohistochemical staining– For the immunohistochemical staining analyses, osteoclasts were fixed with 4% paraformaldehyde, permeabilized, and stained with the indicated specific antibodies, followed by Alexa594-conjugated secondary antibodies and Alexa488-labeled phalloidin (Molecular Probes). The osteoclasts with multiple nuclei (>3) were quantified. Images were captured using an IX-81 fluorescent microscope equipped with a confocal microscopy DSU unit (Olympus, Japan) and were analyzed with the MetaMorph™ software program (Universal Imaging, Molecular Devices, Sunnyvale, CA, USA). The formation of osteoclasts was quantified by capturing and analyzing images using the NIH ImageJ software program (National Institutes of Health, Bethesda, MD) based on TRAP staining of twenty-five fields in each well which were randomly chosen and analyzed.

Real-time PCR analysis– Total cellular RNA from osteoclasts, osteoblasts and bone tissues (proximal tibia after the bone marrow flush and the removal of metaphysial regions) was isolated using the RNeasy kit (QIAGEN, Valencia, CA). The total RNA was then reverse-transcribed into cDNA using the Superscript III RT kit (Invitrogen, Carlsbad, CA). The real-time quantitative PCR analyses were performed using the ABI 7700 sequence detector system with SYBR Green (Applied Biosystems, Foster City, CA, USA). The sequences were amplified for 40 cycles under the following conditions: denaturation at 95°C for 15 s, annealing at 60°C for 30 s, and extension at 72°C for 45 s with primers for the

chemokine receptors as previously reported (17). Gene expression levels were compared to *Gapdh* gene expression by the $2^{-\Delta(Ct)}$ method.

Measurement of cytokines and chemokines– Chemokine CCL5 and CCL9 secretion leveles were determined by ELISA using the MAB4781 and BAF478 antibodies (R&D systems) and the MAB463 and BAF463 antibodies (R&D systems), respectively. The reaction intensities were determined by using HRP-conjugated streptavidin (Chemicon). The cytokine production levels were quantified with a mouse 23-plex multiple cytokine detection system (Bio-Rad. Corp., Hercules, CA, USA) according to the manufacturer's instructions.

Flow cytometry– FITC-, PE-, APC-, PerCP-Cy5.5-, PE-Cy7-, or biotin-conjugated anti–mouse mAbs to CD45.2 (104), CD115 (AFS98), and CD265/RANK (R12-31), and subclass-matched control antibodies were purchased from eBioscience (San Diego, CA). Anti–mouse mAbs to FcγR (2.4G2), Ly6C/6G (RB6-8C5), CD11b (M1/70) and CD19 (1D3) were purchased from BD Pharmingen (San Diego, CA). The flow cytometric analyses were performed using an LSR II flow cytometer with the FACS diva software program (Becton Dickinson) and were analyzed with the FlowJo software program (TreeStar, Ashland, OR). Dead cells were excluded on the basis of the forward and side scatter profiles and propidium iodide staining.

Microcomputed tomography and peripheral quantitative computed tomography– Micro-computed tomography (microCT) scanning was performed on proximal tibiae by μCT-40 (SCANCO Medical AG) with a resolution of 12 μm, and the microstructure parameters were three-dimensionally calculated as previously described (18). The bone scores were measured by peripheral Quantitative Computed Tomography (pQCT) using XCT Research SA+ system (Stratec Medizintechnik GmbH, Pforzheim, Germany). The bone scores and density were measured and analyzed at 1.2 mm below the epiphyseal plate of distal femora. The scores were defined according to the American Society for Bone and Mineral Research standards.

Bone histomorphometry– The unilateral proximal tibiae fixed with ethanol were embedded in glycol methacrylate, and the blocks were cut in 5-μm-thick sections. The structural parameters were analyzed at the secondary spongiosa. For the assessment of dynamic histomorphometric indices, calcein (at a dose of 20 mg/kg body weight) was injected twice (72 hrs interval) to wild-type and *Ccr1*-deficient mice, respectively. The sections were stained with toluidine blue and were analyzed using a semi-automated system (Osteoplan II; ZEISS). The Nomenclature, symbols, and units used in the present study are those recommended by the Nomenclature Committee of the American Society for Bone and Mineral Research (19).

Measurement of TRAP, BALP and collagen-type I N-telopeptides (NTx)– Tartrate-resistant acid phosphatases (TRAP5b) in serum and culture supernatant were measured by the mouse TRAP EIA assay kit (Immunodiagnostic system, Fountain Hills, AZ, USA). In brief, the culture supernatant or diluted serum was applied to an anti-TRAP5b

coated microplate, according to the manufacturer's instruction. The enzymatic activities of bound TRAP were determined with chromogenic substrates. Bone-specific alkaline phosphatase (BALP) levels were measured using the mouse Bone-specific Alkaline Phosphatase ELISA kit (Cusabio Biotech Co Ltd., Wilmington, DE, USA). Collagen-type I N-telopeptides (NTx) were measured by ELISA (SRL, Tokyo).

Collagen-based zymography– Collagen digestion activity was measured by the modified methods, which were based on gelatin-based zymography (20), with some modification for type-I collagen (21,22). In brief, the osteoclasts were gently digested with lysis buffer (150mM NaCl, 50mM HEPES, 5mM EDTA and 10% NP-40 with Halt protease inhibitor cocktail, pH 7.5). The lysates were separated by SDS-PAGE on a 10% polyacrylamide gel with porcine type-I collagen (1 mg/ml , Nitta Gelatin Inc., Osaka, Japan) under chilled conditions. The gel was washed with denaturation buffer (Tris-buffered saline (150mM NaCl, 25mM Tris-HCl, pH 7.4, supplemented with 2.5% Triton-X100) and then subjected to zymography for 18–24 h at 37 °C in zymography developing buffer (Tris-buffered saline, supplemented with 1mM $CaCl_2$, 1μM $ZnCl_2$, and 0.05% Brij-35). The signals were detected using Coomassie Brilliant Blue solution (Wako Pure Chemicals, Osaka, Japan).

Immunoblot analysis. Total cell lysates were isolated, separated by SDS-PAGE, and electrotransferred onto Immobilon-P PVDF membranes (Millipore). The membrane was blocked by 5% BSA in TBST (150mM NaCl, 25mM Tris-HCl (pH 7.4) supplemented with 0.1% Tween 20), and was incubaled with rabbit anti-ATF4 pAb (1/2000), followed by HRP-conjugated anti rabbit IgG (1/10000). The signals were detected using an ECL chemiluminescence substrate (Amersham Biosciences, Piscataway, NJ). The quantitative analysis of blots were normalized using the lumino image analyzer LAS-4000 (Fujifilm Corporation, Japan)

Statistics- Data are presented as the mean ± SEM for the indicated number of independent experiments. Statistical significance was determined with post-hoc test of one-factor factorial ANOVA (**Fig.3E**, **Fig.6D,** and **Fig.7B-C**), the Wilcoxon Mann-Whitney *U*-test (non-parametric analysis, **Fig.2C,** and **Fig.6C**), and S*tudent's t*-test (other Figures) using the KaleidaGraph® 4.0 software programs (Synergy Software, Reading, PA, USA). Differences with a p-value of less than 0.05 was considered to be statistically significant (* and # indicate upregulation and downregulation, respectively). NS: not significant.

Results

CCR1-deficient mice exhibit osteopenia.

To understand the functions of CCR1 in bone metabolism, we investigated the bone mineral density in *Ccr1*$^{-/-}$ mice. A peripheral quantitative computed tomography (pQCT) analysis showed a significant reduction in bone mineral density in cancellous bone in *Ccr1*$^{-/-}$ mice compared to wild-type mice (**Fig.1A**). There were no significant differences between bone mineral density in the cortical bone at the

metaphysial (**Fig.1A**) and diaphysial regions (data not shown) between *Ccr1*-deficient and wild-type mice. In *Ccr1*$^{-/-}$ mice, a microCT analysis indicated decreased cancellous bone tissue at the metaphysical region (**Fig.1B**). An analysis of bone histomorphometrics confirmed a significant decrease of bone volume (BV/TV) at the metaphysial region of *Ccr1*$^{-/-}$ mice. This was associated with a diminished number of trabeculae (Tb.N), increased trabecular bone separation (Tb.Sp), and no significant changes in trabecular bone thickness (Tb.Th), thus indicating that *Ccr1*-deficient mice have sparse trabeculae (**Fig.1C**). We examined the effect of *Ccr1*-deficiency on the function of osteoblasts and osteoclasts in bone morphometry (**Fig.1D-F**). The morphological analyses revealed that *Ccr1*$^{-/-}$ mice have a significantly reduced number of osteoblasts (Ob.S/BS.) (**Fig.1F**). *Ccr1*$^{-/-}$ mice exhibited extremely low values of osteoid surface (OS/BS) and osteoid volume (OV/BV) compared to wild-type mice (**Fig.1D**). Notably, *Ccr1*$^{-/-}$ mice showed a significant decreases in the mineral apposition rate (MAR), mineralized surface (MS/BS), and bone formation rate (BFR/BS) (**Fig.1D**), which were calculated based on calcein administration (representative pictures are shown in **Fig.1E**). In addition, the number of osteocytes per area was significantly reduced in *Ccr1*$^{-/-}$ mice (**Fig.1G**). These results indicate that *Ccr1*$^{-/-}$ mice have impaired bone formation. **Figure.1F** summarizes the bone morphometric parameters associated with bone resorption. *Ccr1*$^{-/-}$ mice have significantly decreased osteoclast numbers (N.Oc./B.Pm) and osteoclast surface area (Oc.S/BS), and an eroded surface (ES/BS). These findings indicate that *Ccr1*$^{-/-}$ mice have diminished osteoclast function. Taken together, the morphometric analyses suggests that the bone phenotype in *Ccr1*-deficient mice exhibit osteopenia with low bone turnover, which is most likely due to the diminished function of osteoblasts and osteoclasts.

Impaired osteogenesis and osteoclastogenesis in the bone tissue of Ccr1-deficient mice.

To elucidate the status of osteoblasts and osteoclasts in bones of *Ccr1*$^{-/-}$ mice, we compared the transcriptional levels of osteoclast- and osteoblast-related markers in the proximal tibiae of wild-type and *Ccr1*$^{-/-}$ mice. The analyses of osteoblast-related markers, such as bone-specific transcriptional factors (*Runx-2, Atf4* and *Osterix*) (23-25) and bone matrix proteins (*Collagen1a1, Osteonectin, Osteopontin* and *Osteocalcin*), revealed that the expression levels of *Runx2* and *Atf4* were dramatically upregulated in *Ccr1*$^{-/-}$ mice than in wild-type mice (**Fig.2A**). However, there were no significant changes in the expression levels of *Osterix*. Early markers for osteoblast differentiation, including *Collagen1a1*, *Osteonectin* and *Osteopontin*, were significantly upregulated. *Osteocalcin* expression, a marker for mature osteoblasts, was significantly downregulated in *Ccr1*$^{-/-}$ mice. These results suggest that osteoblasts in *Ccr1*-deficient mice are retained in an immature state due to the overexpression of *Runx-2* and *Atf4* by osteoblasts, which is also consistent with the significant reduction in number of osteocytes in *Ccr1*$^{-/-}$ mice. Constitutive *Runx-2* overexpression in

osteoblasts results in maturation arrest in osteoblasts and in a reduced number of osteocytes (25). The serum levels of bone-specific alkaline phosphatase (BALP) in *Ccr1*-deficient mice were significantly decreased (**Fig.2C**).

The expression levels of markers related to osteoclast differentiation, revealed attenuated transcription levels of *TRAP5b* and *cathepsin K* in *Ccr1*$^{-/-}$ mice (**Fig.2B**). In addition, *Ccr1*$^{-/-}$ mice exhibited significantly decreased levels of serum TRAP (26) and collagen-type I N-telopeptides (NTx) (27,28) (**Fig.2C**). This finding is consistent with diminished osteoclastic bone resorption in *Ccr1*$^{-/-}$ mice. These observations led us to assess the RANK-RANKL axis, a key signaling pathway in osteoblast-osteoclast interactions that regulates osteoclast differentiation and function. Interestingly, the analyses revealed that both *Rank* and *Rankl* were downregulated (**Fig.2D**), thus implying that CCR1 is involved in the regulation of the RANK-RANKL axis. Considering the fact that *Ccr1*$^{-/-}$ mice exhibit osteopenia with low bone turnover, these bone cell marker expression levels suggest that CCR1 is heavily involved in the differentiation and function of osteoblasts and osteoclasts as well as in the cellular interactions between these cell types.

CCR1 signaling is important in the maturation and function of osteoblasts.

To further corroborate the necessity of CCR1 in osteoblast maturation and function, we examined the formation of mineralized nodules *in vitro* by osteoblastic cells isolated from bone marrow of wild-type and *Ccr1*$^{-/-}$ mice. Mineralized nodule formation in osteoblastic cells isolated from *Ccr1*$^{-/-}$ mice was markedly abrogated compared to wild-type osteoblastic cells (**Fig.3A**). We next investigated the time-course expression profiles of osteoblastic markers in this *in vitro* culture system and compared them between wild-type and *Ccr1*$^{-/-}$ mice (**Fig.3B**). In wild-type mice, *Runx2* exhibited the highest levels of expression at day 14, but was drastically downregulated at day 21, during the mineralization stage. However, an inverse *Runx2* expression pattern was observed in CCR1-deficient osteoblastic cells, in which the levels of expression were markedly suppressed in the early stages (days 0 and 14), and was then significantly upregulated at day 21, reaching the levels present in wild-type mice. *Osterix* expression was highly upregulated at day 21 in wild-type mice, whereas its expression in CCR1-deficient osteoblastic cells was sustained at an intermediate level between the lowest and the highest levels in wild-type mice, overall resulting in a lower expression levels than in wild-type mice at day 21. These inverted expression patterns were also consistently observed, especially at day 21, with other osteoblastic markers, including *Atf4, Caollagen1a1, Osteonectin, Osteopontin* and *Osteocalcin*. Similarly, the expression pattern of ATF4 was also confirmed by a Western blot analysis (**Fig3C**). These observations indicated that CCR1 deficiency severely affected the temporal expression of osteoblastic markers, resulting in the impaired differentiation and maturation of osteoblasts. Because CCR1

signaling is activated by several cross-reactive chemokines (CCL4, CCL5, CCL9 and CCL11), we next compared the levels of these chemokines in wild-type and CCR1-deficient osteoblastic cells. We observed significantly diminished expression levels of these chemokines in *CCR1*-deficient osteoblastic cells (**Fig.3D**). A test on the effects of neutralizing antibodies against various chemokines including CCR1 ligands, revealed the role of each chemokine in mineralized nodule formation by osteoblastic cells. The neutralizing antibodies against CCL4, CCL5, CCL9, and CCL11 significantly reduced the number of mineralized nodules in osteoblastic cells, although the antibodies against CCL2 and CCL3 did not inhibit the numbers completely (**Fig.3E**). Pertussis toxin (PTX), an inhibitor of G*i*-protein-coupled receptors involved in chemokine signaling, inhibited mineralized nodule formation in a dose-dependent manner. In further support of these findings, we observed similar temporal changes in the transcriptional levels of osteoblastic markers in wild-type osteoblastic cultures treated with an anti-CCL9 antibody, compared to *Ccr1*$^{-/-}$ osteoblastic cells (Supplemental Fig.2). These results suggest that CCR1 signaling mediated by its ligands (CCL4, CCL5, CCL 9, and CCL11) play an essential role in mineralized nodule formation.

Lack of chemokine receptor CCR1 causes impaired osteoclast differentiation and bone-resorbing activity

To elucidate the roles of CCR1 in osteoclast differentiation, we analyzed the differentiation potency of osteoclast precursors derived from *Ccr1*$^{-/-}$ mice (**Fig.4A**). Osteoclast precursors from *Ccr1*-deficient mice markedly abrogated multinucleation with defective actin ring formation (**Fig.4A**, yellow arrows) compared to precursors from wild-type mice, which generated a large numbers of osteoclasts with multinucleation and well-organized actin ring formation at the cell periphery. The histograms of the osteoclast area and number of nuclei per cell as well as TRAP-positive areas reveal the presence of impaired cellular fusion and differentiation in *Ccr1*-deficient osteoclasts (**Fig.4B**). We further investigated the activity of bone resorption in *Ccr1*-deficient osteoclasts (**Fig.4C**). Few resorption pits were observed in *Ccr1*$^{-/-}$ osteoclasts by scanning electron microscopic examination, in contrast to obvious resorption pits with well-digested collagen fibers detected in wild-type osteoclasts. This observation was also confirmed by collagen zymography demonstrating that *Ccr1*$^{-/-}$ osteoclasts failed to digest type-I collagens (**Fig.4D**).

Furthermore, the transcriptional levels of osteoclastic differentiation markers were investigated in the osteoclast culture system. *Rank* and its downstream targets *Nfat-c1,* other markers such as *c-fos, Trap, CathepsinK, Atp6v0d2, integrin alpha V* and *integrin beta 3* were markedly downregulated in *Ccr1*-deficient cells whereas *S1P*$_1$ and *Irf-8* were upregulated (**Fig.5A**). We next examined whether the downregulation in RANK expression *in vivo* (see **Fig.2D**) and *in vitro* (**Fig.5A**) directly correlated with the reduction in RANK-expressing osteoclast precursors. The

cellular profiles of osteoclast precursors by a flow cytometric analysis revealed that the *Ccr1*$^{-/-}$ mice had lower numbers of CD45^{+}CD11b^{+}CD115^{+} myeloid-lineage precursors compared to wild-type mice (**Fig.5B**). In addition, the subpopulations of osteoclast precursors, which are categorized into CD11b^{hi} (R1) and CD11b^{lo} (R2), were marked reduced in the R2 subpopulation in CCR1-deficient cells. Because the R1 and R2 subpopulations reportedly express higher and lower levels of RANK, respectively(29), a reduction in the R2 subpopulation likely contributed to reduced expression of osteoclast markers in CCR1-deficient osteoclastic cells. Importantly, our observation is also consistent with a previous work reporting that RANK^{lo} precursors are required for cellular fusion (29).

CCR1 signaling is involved in osteoclast differentiation.

To further explore the role of CCR1 signaling in osteoclast differentiation, we next examined the expression levels of chemokine receptors during osteoclastogenesis using an *in vitro* culture system. CCR1 was expressed in the course of the osteoclastogenesis, with the highest levels of expression at day 4 after culture (10-12), whereas other chemokine receptor CCR2 was gradually downregulated during this culture period (30) (**Fig.6A**). Immunohistochemical staining revealed that CCR1 was highly expressed on the multinuclear osteoclasts (Supplemental Fig.3). The expression profiles of CCR ligands in this *in vitro* osteoclast culture system revealed that ligands specific for CCR1, such as *Ccl5* and *Ccl9*, had a relatively higher levels of expression than other ligands, and appeared to be regulated depending on the maturation stages of the osteoclasts. *Ccl5* was preferentially expressed at day 4, a stage of mononuclear pre-osteoclasts, while multinuclear osteoclasts predominantly produced *Ccl9* at later times (**Fig.6B**). These regulated transcriptional patterns of *Ccl5* and *Ccl9* were also confirmed by the analysis of protein expression levels in cultured media (**Fig.6C**). These observations suggested that the interaction between CCR1 and its ligands, CCL5 and CCL9 could be involved in osteoclast differentiation.

We verified this hypothesis by culturing osteoclast precursors in the presence of neutralizing antibodies against CCL5 and CCL9. Blockade of either ligand resulted in a partial inhibition of osteoclast formation in a dose-dependent manner. Similarly, simultaneous treatment with neutralizing antibodies against CCL5 and CCL9 induced synergistic inhibitory effects (**Fig.6D**). Furthermore, pertussis toxin (PTX) treatment blocked osteoclastogenesis to the basal levels. Notably, we found no CCL3 production by ELISA or any inhibitory osteoclastogenesis effects using an anti-CCL3 antibody (data not shown), although CCL3 is thought to play an essential role in inflammation-related osteoclastogenesis in humans (4,7,31,32). These findings indicate that CCR1 is essential for osteoclast differentiation, and CCL5 and CCL9 are the likely candidate ligands that participate in the CCR1 axis.

CCR1 is involved in the RANK–RANKL axis and induces the impaired osteoclastogenesis

Because osteoclast differentiation is critically regulated by the signals through RANK-RANKL axis, we investigated the transcriptional level of *Rankl* in *Ccr1*$^{-/-}$ osteoblastic cells. The cells expressed significantly lower levels of RANKL compared to wild-type osteoblastic cells (**Fig.7A**). We next performed co-cultures of pre-osteoclasts with layers of osteoblastic cells by reciprocal combinations of these two cell populations from wild-type and *Ccr1*$^{-/-}$ mice. As expected from the reduced *Rankl* expression, a significantly reduced number of osteoclasts were formed from co-culture with *Ccr1*$^{-/-}$ osteoblastic cells compared to wild-type osteoblastic cells (**Fig.7B**). In the presence of PTX, wild-type osteoblastic cells also failed to generate substantial numbers of osteoclasts (**Fig.7B**). *Ccr1*$^{-/-}$ osteoclast precursors did not form differentiated osteoclasts even in the presence of wild-type-derived osteoblasts (**Fig.7C**), as is consistent with our observations in Figure 4. These observations suggest that the CCR1 chemokine receptor, which is expressed by both osteoblasts and osteoclasts, plays a critical role on osteoblast–osteoclast communication through the regulation of the RANK and RANKL expression.

Discussion

Pathological findings postulate that chemokines and chemokine receptors are involved in bone remodeling (9-13). Among these receptors, CCR1 appears to be an important molecules involved in bone metabolism (9). We used *Ccr1*$^{-/-}$ mice to investigate whether CCR1 affects bone metabolism. Our findings have demonstrated that a CCR1-deficiency affects the differentiation and function of both osteoblasts and osteoclasts, and also causes osteopenia.

Our bone histomorphometric study in *Ccr1*$^{-/-}$ mice clearly demonstrated impaired osteoblast differentiation and function (**Fig.1D-G**). The bone tissues in *Ccr1*$^{-/-}$ mice exhibited downregulation of *osteocalcin*, which is a marker for mature osteoblasts, whereas the expression of *Osteonectin* and *Osteopontin*, which are markers for early osteoblasts, were upregulated in the bones of these mice (**Fig.2A**). Significantly, *Ccr1*$^{-/-}$ osteoblastic cells exhibited much less potency to generate mineralized tissues (**Fig.3A**). These results suggest that the deficiency of CCR1 results in arrested osteoblast maturation and defective osteoblast function. Previous reports have demonstrated that the sustained expression of *Runx2* in osteoblasts inhibits their terminal maturation and causes osteopenia with a reduction in the number of osteocytes (25,33). Consistent with these findings, bone tissues specimens from *Ccr1*$^{-/-}$ mice exhibited a higher expression level of *Runx2* and a reduced number of osteocytes (**Fig.3G**). These findings suggest that osteopenia in *Ccr1*$^{-/-}$ mice is due to impaired osteoblastic function via *Runx2* upregulation. Our findings in *Ccr1*$^{-/-}$ osteoblastic culture supportively demonstrated that an inverse temporal expression level of osteoblastic transcriptional factors, such as *Runx2, Atf4* and *Osterix* could be related to the disordered expressions of bone matrix proteins,

thus resulting in impaired bone mineral deposition (**Fig.3B**).

Furthermore, treatment with neutralizing antibodies against CCR1 ligands (e.g., CCL4, CCL5, CCL9 and CCL11) significantly inhibited mineral deposition (**Fig.3E**) and osteoblastic protein expression (supplemental Fig.2) in osteoblastic cells isolated from wild-type mice. These observations indicate that CCR1-mediated signaling is essential for osteoblast differentiation and function. Although we detected substantial levels of various chemokine ligands (CCL4, CCL5, CCL9 and CCL11) in osteoblastic cells, these levels were greatly reduced in cells isolated from *Ccr1*$^{-/-}$ mice (**Fig.3D**). This observation implies a chemokine-dependent amplification loop by which a given chemokine signaling sustains or amplifies the expressions of its participating ligands and receptors, which has been previously reported in several contexts. For instance, the activation of CD14^{+} monocytes form a CCR2-CCL2 axis-dependent amplification loop ultimately leads to fibrosis (34). Several other studies have reported that macrophage infiltration in injured tissue is mediated by a CCR1-mediated loop (35-37) and a CCR5–CCL5 loop (38). Reports of renal inflammatory signals and abdominal inflammation have described CCR7–CCL19/CCL21 (39) and CCR8–CCL1 loops (17), respectively. Therefore, the CCR1-mediated loop is likely to be involved in osteoblast differentiation, function and cellular interactions that regulate bone metabolism. Possible roles of the CCR1-mediated loop in osteoblast differentiation and function suggest that changes in the bone marrow microenvironment by a CCR1–deficiency affected the osteoblastic lineage and/or the inter-cellular regulation of osteoblast differentiation and function. CCR1 conventional knock-down seems to have affected many cell types that express CCR1, affecting the_bone marrow microenvironment, which regulates whole process of osteoblast differentiation and function. Our *in vitro* experiments did not successfully retrieve this point. Nevertheless, the present experiments have confirmed an essential role for CCR1-mediated signaling in osteoblastic cells. The expression and possible roles of CCR1 in osteoclast lineage cells have been reported by several studies (4,10,11). We observed the upregulation of *Ccr1* expression and downregulation of *Ccr2* during cultured osteoclastogenesis (**Fig.6A**). The bone histomorphometric analyses demonstrated impaired osteoclast differentiation and function in *Ccr1*$^{-/-}$ mice (**Fig.1F**). In addition, we observed impaired bone resorption activity by osteoclasts isolated from *CCR1*$^{-/-}$ mice (**Fig. 4B-C**). A potential reason for the impaired bone resorption is due to defects in osteoclast differentiation. Indeed, the flow cytometric analyses revealed that the component of CD11b^{+}CD115^{+} myeloid-lineage precursors in *Ccr1*$^{-/-}$ mice are drastically changed; this population of cells lacked the RANK^{lo} CD11b^{lo} subpopulation, which are required for cellular fusion (29) (**Fig.5B**). Recent live observation of calvarial bone marrow by two-photon microscopy clarified the roles of chemoattractant S1P$_1$ (sphingosine-1-phosphate

1) and its receptors in the migration of osteoclast precursors to the bone surface (40). Therefore, it is indeed intriguing to speculate that elevated levels of *S1P$_1$* expression in *Ccr1*$^{-/-}$ osteoclasts (**Fig.1F**) reduced the supply of osteoclast precursors from peripheral circulation in the bone marrow to the bone surface. Further investigation will reveal whether the CCR1 axis is involved in the chemotactic migration of osteoclast precursors to the bone surface.

One of the possible reasons for osteoclast dysfunction in *Ccr1*$^{-/-}$ mice may be diminished signaling along the RANK–RANKL axis. The downregulation of both *Rank* and *Rankl* mRNA was observed in the bone tissue of *Ccr1*$^{-/-}$ mice (**Fig.2D**). Cultured osteoblastic cells and osteoclasts isolated from *Ccr1*$^{-/-}$ mice exhibited remarkable reductions in *Rank* and *Rankl* expression levels, respectively (**Fig.7B and Fig.5B**). Furthermore, *Ccr1*-deficient osteoclasts had discouraged the levels of osteoclastic maturation markers such as *c-fos*, *Nfatc1*, *Cathepsin K*, and several integrins (**Fig.5A**). These results suggest that CCR1-mediated signaling controls the RANK–RANKL axis through the regulation of both osteoblasts and osteoclasts. Our intercross co-cultures of pre-osteoclasts with osteoblastic cells from wild-type and *Ccr1*$^{-/-}$ mice obviously demonstrated an impaired interaction between these two cell types, resulting in the impaired induction of functional mature osteoclasts (**Fig.7B-C**). These findings, interestingly, support the idea that the chemokines produced by the osteoblasts and osteoclasts that stimulate CCR1-mediated signaling, could be categorized as a putative ”bone-coupling factors” (41), which mediate the crosstalk between osteoclasts and osteoblasts to maintain bone remodeling.

Our data imply that the regulatory mechanism of *Rankl* expression is associated with osteoblast maturation. Runx2 reportedly induce a low steady-state level of *Rankl* expression, and is also required for the stimulatory effect of vitamin D_3 on *Rankl* transcription possibly by condensing or decondensing the chromatin structure(42). It is possible that the inverse-temporal *Runx2* expression in CCR1-deficient mice is causative of the down-regulation of *Rankl*, due to a reduced cellular response to bone-targeted hormones such as vitamin D_3 and PTH. However, a more direct role of CCR1-mediated signaling on *Rankl* transcription remains to be elucidated.

CCR1-mediated signaling pathways on both osteoblasts and osteoclasts raise important questions on how the several members of murine chemokine ligands for CCR1 (in rodents, CCL3, CCL4, CCL5, CCL6, CCL8, CCL9 and CCL11) (43) distinguish the downstream signaling pathways, despite sharing the same CCR1 receptor. Each chemokine may possess specific regulatory control for binding to the receptor and inducing a specific cellular response. For example, the osteoclasts may have a distinct intrinsic signaling adaptor protein for cellular response, as well as the adaptor protein FROUNT for CCR2-mediated signaling (44). It has also been demonstrated that the spatio-temporal expression of chemokine receptors and their ligands may relay chemokine signaling and

sequential output that regulate bone metabolism. This is related to several findings in this study, including the distinct temporal expression patterns of different ligands as observed in **Fig.6B-C**, and supplemental Fig.1, the chemokine-dependent amplification loop, and the possible chemokine-mediated cellular interaction. Further studies are warranted to investigate the intracellular signaling pathways downstream of each chemokine receptor.

Our current results also support the concept that chemokine receptor antagonists are potentially novel therapeutic candidates for the treatment of patients with certain inflammatory bone diseases. Several reports suggest that CCL3 promotes pathological bone destruction by excessively triggering osteoclast activation (2,4,7,31,32). However, we were unable to detect increased CCL3 production by cultured osteoclasts (**Fig.6B-C**, and data not shown), suggesting that physiological osteoclastogenesis is primarily maintained by CCL9 rather than CCL3. It is probable that proinflammatory CCL3 overcomes the physiological process of osteoclastogenesis by CCL9 expression and signaling, thereby inducing ectopic osteoclastogenesis that causes bone destruction mediated by T lymphocyte-mediated activation (45). Alternatively, the species differences between rodents and humans must be considered; CCL9 is described only in rodents, and the putative human homologue is predicted to be CCL15 and CCL23 (46), which are potent osteoclastogenesis mediators in humans (47). It is therefore worthwhile to dissect the distinct roles of chemokine signaling in both the pathological and physiological contexts, which would provide novel information that may help researchers identify new therapeutic targets.

In conclusion, the present observations provide the first evidence for the physiological roles of CCR1-mediated chemokines in the bone metabolism. Further studies on chemokine receptors in the bone metabolism will enable the targeted development of new therapeutic strategies for the treatment of patients with bone destruction diseases and osteoporosis.

Acknowledgments

Acknowledgments: The author thanks to Dr. Taeko Dohi, Dr. Harumi Suzuki, Dr. Yasuhiro Natori, and Ms Mikiko Uwano (IMCJ), Philip M. Murphy (NIH), and T. Sakai for valuable advices and supports. The author is grateful to Dr. Takuro Shimbo and Dr. Tetsuya Mizoue (IMCJ) for statistical supports.

Financial Supports: A.H. was also supported by grants from the Japan foundation of Cardiovascular Research (2006) and from the Naito foundation (2005); Yu.M. was supported by grant “H21-nanchi-097” from the Ministry of Health, Labor and Welfare; A.Y. and Ta. I were supported by the grant aid from the Japanese Ministry of Education, Global Center of Excellence (GCOE) Program, “International Research Center for Molecular Science in Tooth and Bone Diseases”; Ta. I. was also supported by The Takeda Science Foundation, The Mochida Memorial Foundation for Medical and Pharmaceutical Research and a Grant-in-Aid for Scientific Research from the Japan Society for the Promotion of Science (21659426); K.M. was supported by Solution Oriented Research for Science and Technology and by the Japan Science and Technology Corporation.

Author Contributions: A.H. performed the

whole research in support of Ta.I., S.U., S.H., Yo.M.; A.H., Ta.I., M.Y., A.Y., K.M., and K.Y. contributed to the research design; A.Y directed and organized the bone morphologic analysis; Ta.I., Yu.M., and M.I. supported the bone morphologic analysis; S.U., and K.M. contributed to the flow cytometric analyses and provided the gene-deficient mice; M.M., and K.S., contributed to the electron microscopic analyses and the research equipments; To.I. provided the anti-CX3CL1 antibodies and the related reagents; T.K. and K.Y. supervised the whole project; and A.H and Ta.I. designed the detail of experiments and wrote the paper.

Footnotes

This work was mainly supported by a grant "H19-nano-012" from the Ministry of Health, Labor and Welfare to K.Y; in parts by a research fellowship of the Japan Society for the Promotion of Science for Young Scientists (2007-2009) to A.H.

The Abbreviation used are : BALP, bone-specific alkaline phosphatase(s); CCL, C-C chemokine ligands(s); CCR, C-C chemokine receptor(s); MCP-1, macrophage chemoattractant protein-1; M-CSF, macrophage-colony stimulation factor; MIP-1, macrophage inflammatory protein-1; pQCT, peripheral quantitative computed tomography; PTX, pertussis toxin from *Bordetella pertussis*; RANK, receptor activator of NF-κB; RANKL, receptor activator of NF-κB ligand; RANTES, regulated upon activation normal T expression and secreted; TRAP, tartrate-resistant acid phosphatase(s).

Keywords - bone metabolism, bone resorption, cell fusion, calcification, chemokines, chemokine receptors, CCL5, CCL9, CCR1, multinucleation, osteoclasts, osteoblasts, osteolysis, osteopenia.

References

1. *Charo, I. F., and Ransohoff, R. M. (2006) N Engl J Med **354**(6), 610-621*
2. *Oba, Y., Lee, J. W., Ehrlich, L. A., Chung, H. Y., Jelinek, D. F., Callander, N. S., Horuk, R., Choi, S. J., and Roodman, G. D. (2005) Exp Hematol **33**(3), 272-278*
3. *Kim, M. S., Magno, C. L., Day, C. J., and Morrison, N. A. (2006) J Cell Biochem **97**(3), 512-518*
4. *Menu, E., De Leenheer, E., De Raeve, H., Coulton, L., Imanishi, T., Miyashita, K., Van Valckenborgh, E., Van Riet, I., Van Camp, B., Horuk, R., Croucher, P., and Vanderkerken, K. (2006) Clin Exp Metastasis **23**(5-6), 291-300*
5. *Haringman, J. J., Smeets, T. J., Reinders-Blankert, P., and Tak, P. P. (2006) Ann Rheum Dis **65**(3), 294-300*
6. *Choi, S. J., Cruz, J. C., Craig, F., Chung, H., Devlin, R. D., Roodman, G. D., and Alsina, M. (2000) Blood **96**(2), 671-675*
7. *Han, J. H., Choi, S. J., Kurihara, N., Koide, M., Oba, Y., and Roodman, G. D. (2001) Blood **97**(11), 3349-3353*
8. *Vallet, S., Raje, N., Ishitsuka, K., Hideshima, T., Podar, K., Chhetri, S., Pozzi, S., Breitkreutz, I., Kiziltepe, T., Yasui, H., Ocio, E. M., Shiraishi, N., Jin, J., Okawa, Y., Ikeda, H., Mukherjee, S., Vaghela, N., Cirstea, D., Ladetto, M., Boccadoro, M., and Anderson, K. C. (2007) Blood **110**(10), 3744-3752*
9. *Yang, M., Mailhot, G., MacKay, C. A., Mason-Savas, A., Aubin, J., and Odgren, P. R. (2006) Blood **107**(6), 2262-2270*
10. *Yu, X., Huang, Y., Collin-Osdoby, P., and Osdoby, P. (2004) J Bone Miner Res **19**(12), 2065-2077*
11. *Lean, J. M., Murphy, C., Fuller, K., and Chambers, T. J. (2002) J Cell Biochem **87**(4),*

386-393
12. Okamatsu, Y., Kim, D., Battaglino, R., Sasaki, H., Spate, U., and Stashenko, P. (2004) J Immunol **173**(3), 2084-2090
13. Kominsky, S. L., Abdelmagid, S. M., Doucet, M., Brady, K., and Weber, K. L. (2008) Cancer Res **68**(5), 1261-1266
14. Binder, N. B., Niederreiter, B., Hoffmann, O., Stange, R., Pap, T., Stulnig, T. M., Mack, M., Erben, R. G., Smolen, J. S., and Redlich, K. (2009) Nat Med **15**(4), 417-424
15. Gao, J. L., Wynn, T. A., Chang, Y., Lee, E. J., Broxmeyer, H. E., Cooper, S., Tiffany, H. L., Westphal, H., Kwon-Chung, J., and Murphy, P. M. (1997) J Exp Med **185**(11), 1959-1968
16. Doi, M., Nagano, A., and Nakamura, Y. (2002) Biochem Biophys Res Commun **290**(1), 381-390
17. Hoshino, A., Kawamura, Y. I., Yasuhara, M., Toyama-Sorimachi, N., Yamamoto, K., Matsukawa, A., Lira, S. A., and Dohi, T. (2007) J Immunol **178**(8), 5296-5304
18. Ito, M., Ikeda, K., Nishiguchi, M., Shindo, H., Uetani, M., Hosoi, T., and Orimo, H. (2005) J Bone Miner Res **20**(10), 1828-1836
19. Parfitt, A. M., Drezner, M. K., Glorieux, F. H., Kanis, J. A., Malluche, H., Meunier, P. J., Ott, S. M., and Recker, R. R. (1987) J Bone Miner Res **2**(6), 595-610
20. Liotta, L. A., and Stetler-Stevenson, W. G. (1990) Semin Cancer Biol **1**(2), 99-106
21. Gogly, B., Groult, N., Hornebeck, W., Godeau, G., and Pellat, B. (1998) Anal Biochem **255**(2), 211-216
22. Wilson, M. J., Strasser, M., Vogel, M. M., and Sinha, A. A. (1991) Biol Reprod **44**(5), 776-785
23. Komori, T., Yagi, H., Nomura, S., Yamaguchi, A., Sasaki, K., Deguchi, K., Shimizu, Y., Bronson, R. T., Gao, Y. H., Inada, M., Sato, M., Okamoto, R., Kitamura, Y., Yoshiki, S., and Kishimoto, T. (1997) Cell **89**(5), 755-764
24. Ducy, P., Zhang, R., Geoffroy, V., Ridall, A. L., and Karsenty, G. (1997) Cell **89**(5), 747-754
25. Liu, W., Toyosawa, S., Furuichi, T., Kanatani, N., Yoshida, C., Liu, Y., Himeno, M., Narai, S., Yamaguchi, A., and Komori, T. (2001) J Cell Biol **155**(1), 157-166
26. Delmas, P. D. (1993) J Bone Miner Res **8 Suppl 2**, S549-555
27. Takahashi, M., Kushida, K., Hoshino, H., Ohishi, T., and Inoue, T. (1997) J Endocrinol Invest **20**(3), 112-117
28. Schneider, D. L., and Barrett-Connor, E. L. (1997) Arch Intern Med **157**(11), 1241-1245
29. Arai, F., Miyamoto, T., Ohneda, O., Inada, T., Sudo, T., Brasel, K., Miyata, T., Anderson, D. M., and Suda, T. (1999) J Exp Med **190**(12), 1741-1754
30. Saitoh, Y., Koizumi, K., Sakurai, H., Minami, T., and Saiki, I. (2007) Biochem Biophys Res Commun **364**(3), 417-422
31. Abe, M., Hiura, K., Wilde, J., Moriyama, K., Hashimoto, T., Ozaki, S., Wakatsuki, S., Kosaka, M., Kido, S., Inoue, D., and Matsumoto, T. (2002) Blood **100**(6), 2195-2202
32. Chintalacharuvu, S. R., Wang, J. X., Giaconia, J. M., and Venkataraman, C. (2005) Immunol Lett **100**(2), 202-204
33. Kanatani, N., Fujita, T., Fukuyama, R., Liu, W., Yoshida, C. A., Moriishi, T., Yamana, K., Miyazaki, T., Toyosawa, S., and Komori, T. (2006) Dev Biol **296**(1), 48-61
34. Sakai, N., Wada, T., Furuichi, K., Shimizu, K., Kokubo, S., Hara, A., Yamahana, J., Okumura, T., Matsushima, K., Yokoyama, H., and Kaneko, S. (2006) J Leukoc Biol **79**(3), 555-563
35. Furuichi, K., Gao, J. L., Horuk, R., Wada, T., Kaneko, S., and Murphy, P. M. (2008) J Immunol **181**(12), 8670-8676
36. Ma, B., Zhu, Z., Homer, R. J., Gerard, C., Strieter, R., and Elias, J. A. (2004) J Immunol **172**(3), 1872-1881

37. Shang, X., Qiu, B., Frait, K. A., Hu, J. S., Sonstein, J., Curtis, J. L., Lu, B., Gerard, C., and Chensue, S. W. (2000) Am J Pathol **157**(6), 2055-2063
38. Anders, H. J., Frink, M., Linde, Y., Banas, B., Wornle, M., Cohen, C. D., Vielhauer, V., Nelson, P. J., Grone, H. J., and Schlondorff, D. (2003) J Immunol **170**(11), 5658-5666
39. Coates, P. T., Colvin, B. L., Ranganathan, A., Duncan, F. J., Lan, Y. Y., Shufesky, W. J., Zahorchak, A. F., Morelli, A. E., and Thomson, A. W. (2004) Kidney Int **66**(5), 1907-1917
40. Ishii, M., Egen, J. G., Klauschen, F., Meier-Schellersheim, M., Saeki, Y., Vacher, J., Proia, R. L., and Germain, R. N. (2009) Nature **458**(7237), 524-528
41. Matsuo, K., and Irie, N. (2008) Arch Biochem Biophys **473**(2), 201-209
42. Kitazawa, R., Mori, K., Yamaguchi, A., Kondo, T., and Kitazawa, S. (2008) J Cell Biochem **105**(5), 1289-1297
43. Murphy, P. M., Baggiolini, M., Charo, I. F., Hebert, C. A., Horuk, R., Matsushima, K., Miller, L. H., Oppenheim, J. J., and Power, C. A. (2000) Pharmacol Rev **52**(1), 145-176
44. Terashima, Y., Onai, N., Murai, M., Enomoto, M., Poonpiriya, V., Hamada, T., Motomura, K., Suwa, M., Ezaki, T., Haga, T., Kanegasaki, S., and Matsushima, K. (2005) Nat Immunol **6**(8), 827-835
45. Sato, K., Suematsu, A., Okamoto, K., Yamaguchi, A., Morishita, Y., Kadono, Y., Tanaka, S., Kodama, T., Akira, S., Iwakura, Y., Cua, D. J., and Takayanagi, H. (2006) J Exp Med **203**(12), 2673-2682
46. Votta, B. J., White, J. R., Dodds, R. A., James, I. E., Connor, J. R., Lee-Rykaczewski, E., Eichman, C. F., Kumar, S., Lark, M. W., and Gowen, M. (2000) J Cell Physiol **183**(2), 196-207
47. Rioja, I., Hughes, F. J., Sharp, C. H., Warnock, L. C., Montgomery, D. S., Akil, M., Wilson, A. G., Binks, M. H., and Dickson, M. C. (2008) Arthritis Rheum **58**(8), 2257-2267

Figure Legends

Figure 1. Bone morphometric analyses of CCR1$^{-/-}$ mice. *Panel A* shows the bone mineral density of trabecular and cortical bones in distal femurs as measured by pQCT. *Panel B* shows the microCT images and the quantitative measurements of trabecular bones (Tb.V.) in the distal femurs of wild-type and *Ccr1*$^{-/-}$ mice. (n=10). In *panels C-F*, the bone histomorphometric analyses of distal femurs in wild-type and *CCR1*$^{-/-}$ mice were carried out as described in the experimental procedures. Parameters relating to the trabecular structure (in *panel C*): bone volume per tissue volume (BV/TV), trabecular number (Tb.N.), and trabecular separation (Tb.Sp.). Parameters relating to bone formation (in *panel D*): osteoid volume to bone volume (OV/BV), osteoid surface/bone surface (OS/BS), osteoid thickness (O.Th.), formation rate referenced to bone surface (BFR/BS), mineral apposition rate (MAR), and mineralizing surface per bone surface (MS/BS). The immunofluorescence images of calcein labeling in wild-type and *Ccr1*$^{-/-}$ mice (in *panel E*). Parameters relating to bone resorption (in *panel F*): osteoclast number per bone perimeter (N.Oc./B.Pm), osteoclast surface per bone surface (Oc.S./BS), eroded surface per bone surface (ES/BS), and osteoblast surface per bone surface (Ob.S./BS). The bone histomorphometric analysis data are represented as the mean ± SEM obtained from 6 mice in each group. #, significantly different from wild-type controls, $p<0.05$. In *panel G*: osteocyte numbers per area are represented as the mean ± SEM obtained from 3 mice in each group.

Figure 2. Expression of markers related to osteoblasts and osteoclasts in bones and

sera in wild-type and *CCR1*$^{-/-}$ mice. In *panels A, B and D*, total RNAs were isolated form the proximal tibia of wild-type and *Ccr1*$^{-/-}$ male mice at 8 weeks of age. Realtime Q-PCR revealed the relative expression levels of osteoblast-related mRNAs (*Runx-2*, *Osterix, Atf4, Osteonectin, Osteopontin, Osteocalcin* and *Collagen1α1*, *panel A*) , osteoclast-related mRNA (*Trap5a* and *Cathepsin K*, *panel B*) and RANK/RANKL axis (*Rank* and *Rankl*, *panel D*). Data are expressed as the copy numbers of these markers normalized to *Gapdh* expression (mean ± SEM, n=8). In *panel C*, the levels of serum BALP, TRAP and serum collagen-type1 N-telopeptides (NTx) were measured by ELISA. The bars indicate the mean. Each sample was duplicated. Wild-type and *Ccr1*$^{-/-}$ male mice at 9 weeks of age (n=10 and 6, respectively) were subjected to BALP and TRAP. Wild-type and *Ccr1*$^{-/-}$ male mice at 9–13 weeks of age (n=8 and 6, respectively) were assayed for NTx. #, significantly different from wild-type controls, $p<0.05$. N.D.: not detected.

Figure 3. Impaired mineralized nodule formation in *CCR1*-deficient osteoblastic cells. In *panel A*, osteoblastic cells were cultured from the bone marrow of wild-type and *Ccr1*$^{-/-}$ mice, and then minerals were stained with alizarin red and BALP with chromogenic reagents (shown in blue) (magnification ×100, *left*). Mineral deposition was determined by von Kossa staining (n=6, *right*). In *panel B*, total RNAs were isolated from osteoblastic cells isolated from wild-type (open circles) and *Ccr1*$^{-/-}$mice (filled circles). The realtime Q-PCR analyses examined the relative expression levels of osteoblast-related transcriptional factor mRNAs (*Runx-2*, *Osterix, Atf4)* and osteoblast-related marker mRNAs (*Osteonectin, Osteopontin, Osteocalcin*, and *Collagen1α1*). Data are expressed as the copy numbers of these markers normalized to *Gapdh* expression (mean ± SEM, n=8). In *panel C*, the protein expression levels of the transcriptional factor ATF4 by wild-type and *Ccr1*$^{-/-}$ osteoblastic cells were measured by a Western blot analysis. Osteoblast lysates (10 μg protein per lane) was loaded and separated by SDS-PAGE. The expression levels of ATF4 were normalized to GAPDH expression. In *panel D*, the production of CCR1-related chemokine ligands in the culture media of wild-type and *Ccr1*$^{-/-}$ osteoblastic cells was measured by ELISA (n=5). #, significantly different from wild-type controls, $p<0.05$. In *panel E*, osteoblastic cells were cultured with the indicated neutralizing antibodies against chemokines. The mineral deposition rate was measured by von Kossa staining (n=4). Stained cells cultured with control rat IgG were set as 100%. #, significantly different from between different concentrations of each antibody, $p<0.05$. PTX: pertussis toxin.

Figure 4. Essential roles of CCR1 in multinucleation and bone-resorbing activity. Pre-osteoclastic cells were cultured from the bone marrow of wild-type and *Ccr1*$^{-/-}$ mice. Osteoclasts were induced from the pre-osteoclastic cells by M-CSF and RANKL treatment. In *panel A*, the formation of multinuclear osteoclasts by wild-type and *Ccr1*$^{-/-}$ precursors was visualized by TRAP chromogenic staining (magnification ×400, *upper*). Immunohistochemical staining was carried out using an anti-cathepsin K antibody conjugated with Alexa594 (red). F-actin and nuclei were counterstained by phalloidin–AlexaFluor 488 (green) and hoechst33258 (blue), respectively (Magnification ×640, *bottom*). The yellow arrow indicates multinuclear giant-cells with an impaired actin ring rearrangement, and the red arrows indicate TRAP accumulation. In *panel B*, histograms of the area distribution of multinuclear osteoclasts delimited with phalloidin, and of the number of multinuclear osteoclasts in ***panel A***. Area of TRAP-positive multinuclear (>3 nuclei) giant-cells shown in ***panel A*** (mean ± SEM, n=3). In *panel C*, collagen digestion activity by wild-type and *Ccr1*$^{-/-}$ osteoclasts was measured by

collagen-based zymography. Lanes M, 1, 2–3 and 4–5 indicate the molecular markers, bone marrow-derived macrophage lysates (10 μg protein/lane), wild-type osteoclast lysates (1 and10 μg protein/lane) and *Ccr1*$^{-/-}$ osteoclasts lysates (1 and 10 μg protein/ each lane), respectively. In *panel D*, Pit formation by wild-type and *Ccr1*$^{-/-}$ osteoclasts on bone slice observed by Scanning Electron Microscopy. Magnification: ×1000 (*top*) and ×6000 (*bottom*), respectively.

Figure 5. Osteoclastic impairment by CCR1-deficiency is due to the changes in osteoclastic precursor population. Pre-osteoclastic cells were cultured from the bone marrow of wild-type and *Ccr1*$^{-/-}$ mice. Osteoclasts were induced from the pre-osteoclastic cells by M-CSF and RANKL treatment. In *panel A*, relative expression levels of the osteoclastic differentiation markers (*Rank*, *Nfatc1* transcription factor, *c-fos*, *Trap*, *CathepsinK* protease, H^+-ATPase subunit *ATP6v0d2*, integrins *alphaV* and *beta3*, $S1P_1$ and *Irf-8*) on wild-type (open column) and *Ccr1*$^{-/-}$ (filled column) osteoclasts were measured by a real-time Q-PCR analysis at day 4 after culture (mean ± SEM, n=5). #, significantly different from wild-type controls, $p<0.05$. In *panel B*, expression analysis of RANK in $CD45^+CD11b^+CD115^+$ pre-osteoclastic cells isolated from the bone marrows of wild-type and *Ccr1*$^{-/-}$ mice after 4 days in culture were analyzed by flow cytometry.

Figure 6. CCR1 signaling is involved in osteoclast differentiation. Osteoclastic cells and macrophages were cultured from the bone marrow of wild-type and *Ccr1*$^{-/-}$ mice. Total RNAs were isolated from the cultured cells. The relative mRNA expression levels of chemokine receptors *Ccr1, Ccr2* (*panel A*) and chemokine ligands (*panel B*) during osteoclastogenesis were measured by realtime Q-PCR (mean ± SEM, n=5). * and #, significantly different from day 0 of *Ccr1* and *Ccr2*, respectively, $p<0.05$ in *panel A*. ∗, significantly different from day 0 of culture in each ligand expression, $p<0.05$ in *panel B*. In *panel C*, chemokine levels during osteoclastogenesis were measured by ELISA. BM, bone marrow-derived macrophage; POC, pre-osteoclast (day4); and OC, osteoclast (day14). Bars indicate the mean. In *panel D*, the number of osteoclasts after neutralization of CCL5, CCL9 and their combination in the osteoclastic cultures were scored (mean ± SEM, n=3). #, significantly different between two distinct concentrations of each antibody, $p<0.05$. PTX: pertussis toxin.

Figure 7. CCR1 is involved in the RANK–RANKL axis and induces the impaired osteoclastogenesis. In *panel A*, osteoblastic cells were cultured from the bone marrow of wild-type and *Ccr1*$^{-/-}$ mice. Relative expression levels of *Rankl* by *Ccr1*$^{-/-}$ osteoblasts as measured by realtime Q-PCR (mean ± SEM, n=3). #, significantly different from wild-type controls, $p<0.05$. In *panel B-C*, the number of $TRAP^+$ multinuclear osteoclasts induced by co-culture with osteoblasts. Co-culture with osteoblastic cells isolated from wild-type or *Ccr1*$^{-/-}$ mice (mean ± SEM, duplicated, n=2, *panel B*), and with osteoclast precursors isolated from wild-type or *Ccr1*$^{-/-}$ mice (mean ± SEM, duplicated, n=2, *panel C*). Osteoclast cultures with M-CSF and RANKL without osteoblasts were set as positive control. #, significantly different from co-culture of osteoclasts with wild-type osteoblasts, $p<0.05$.

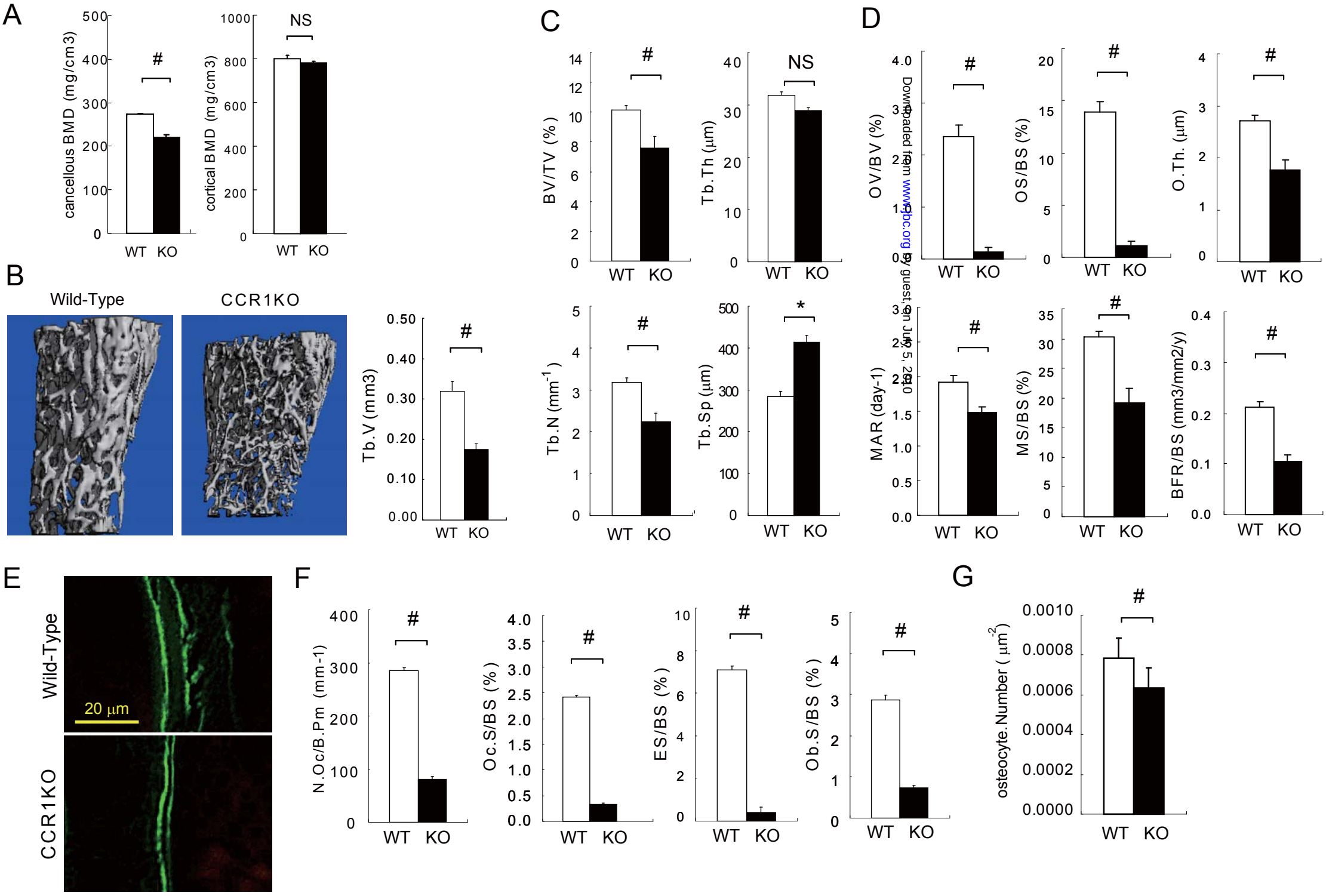

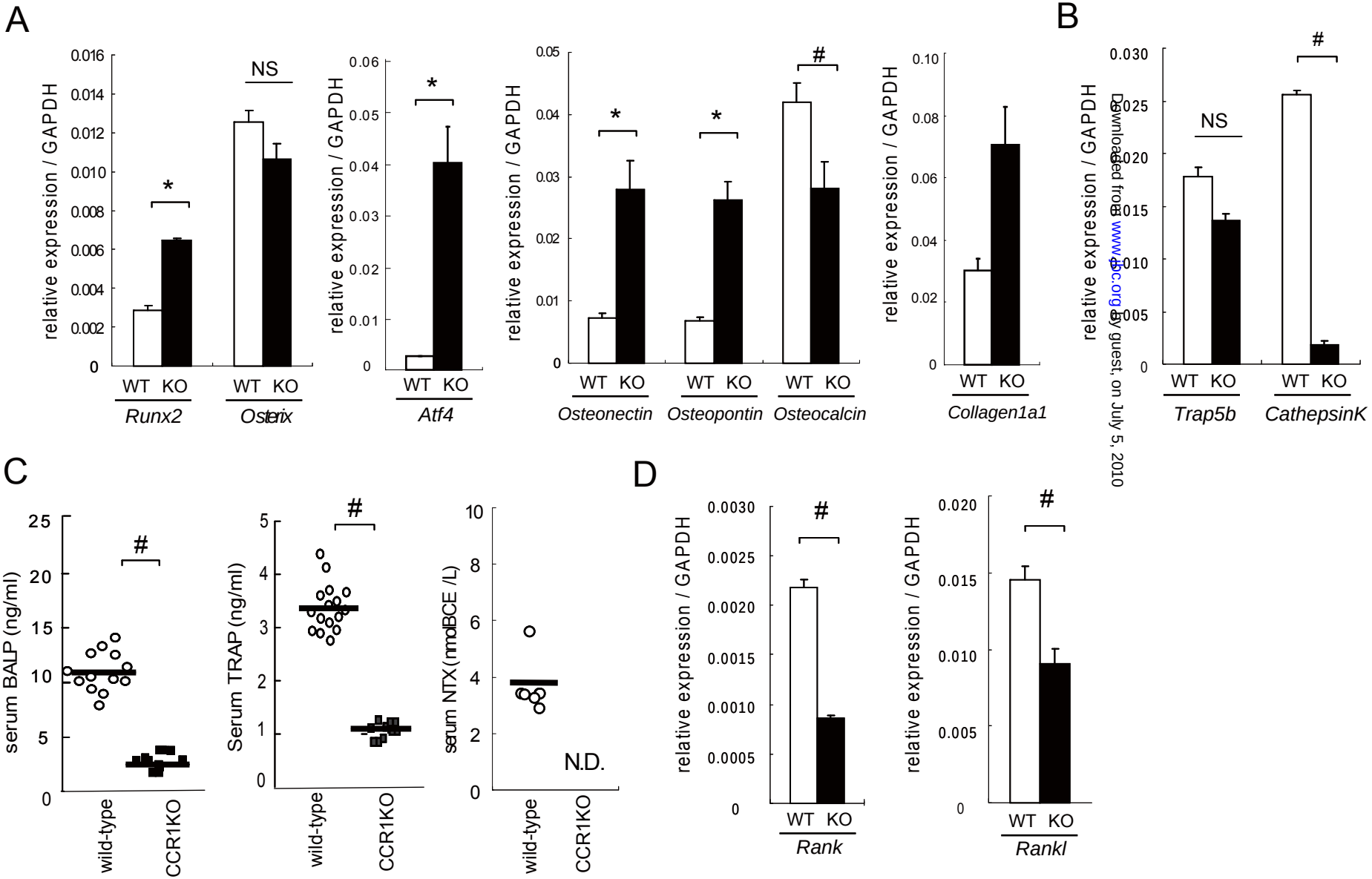

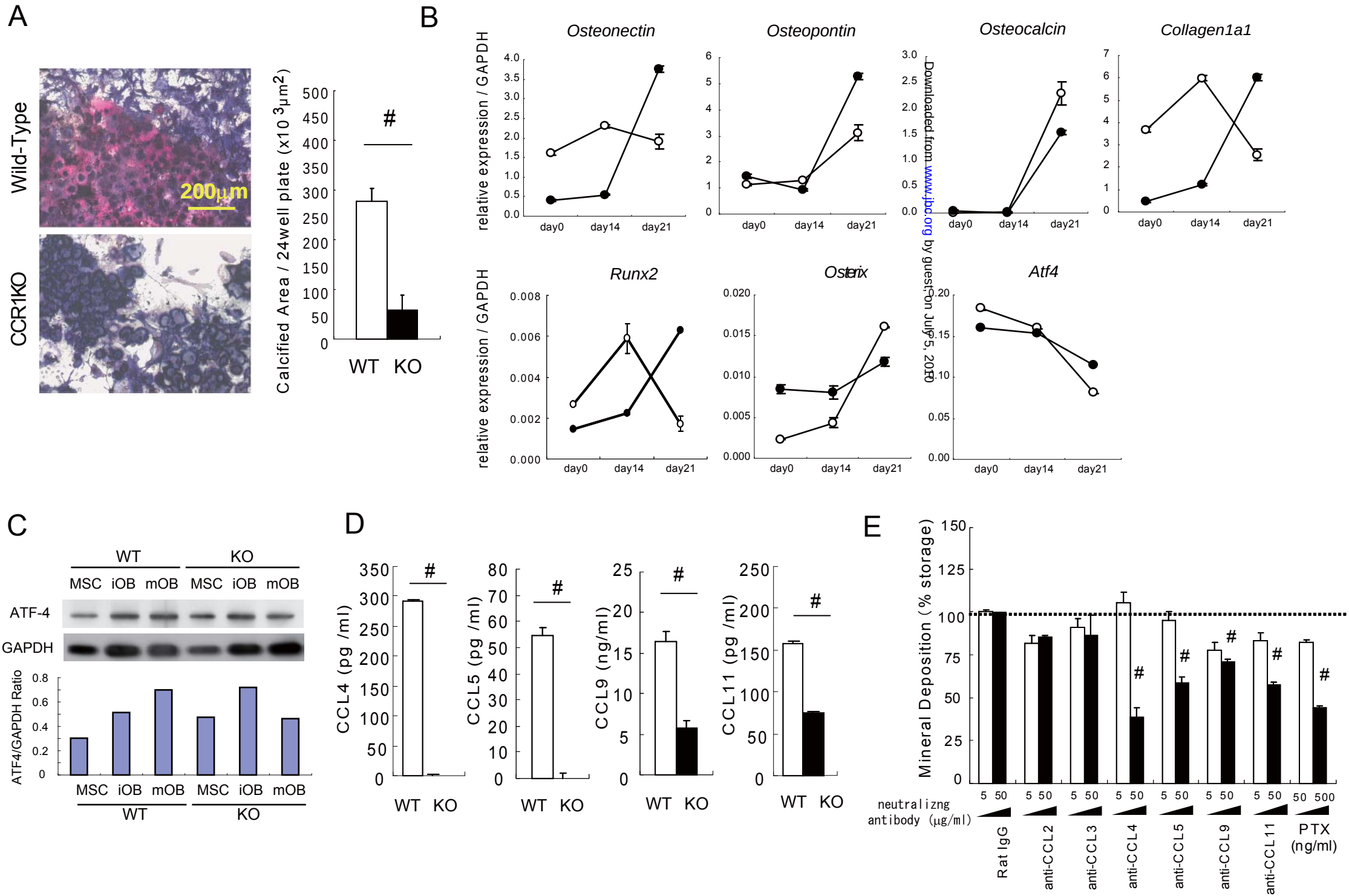

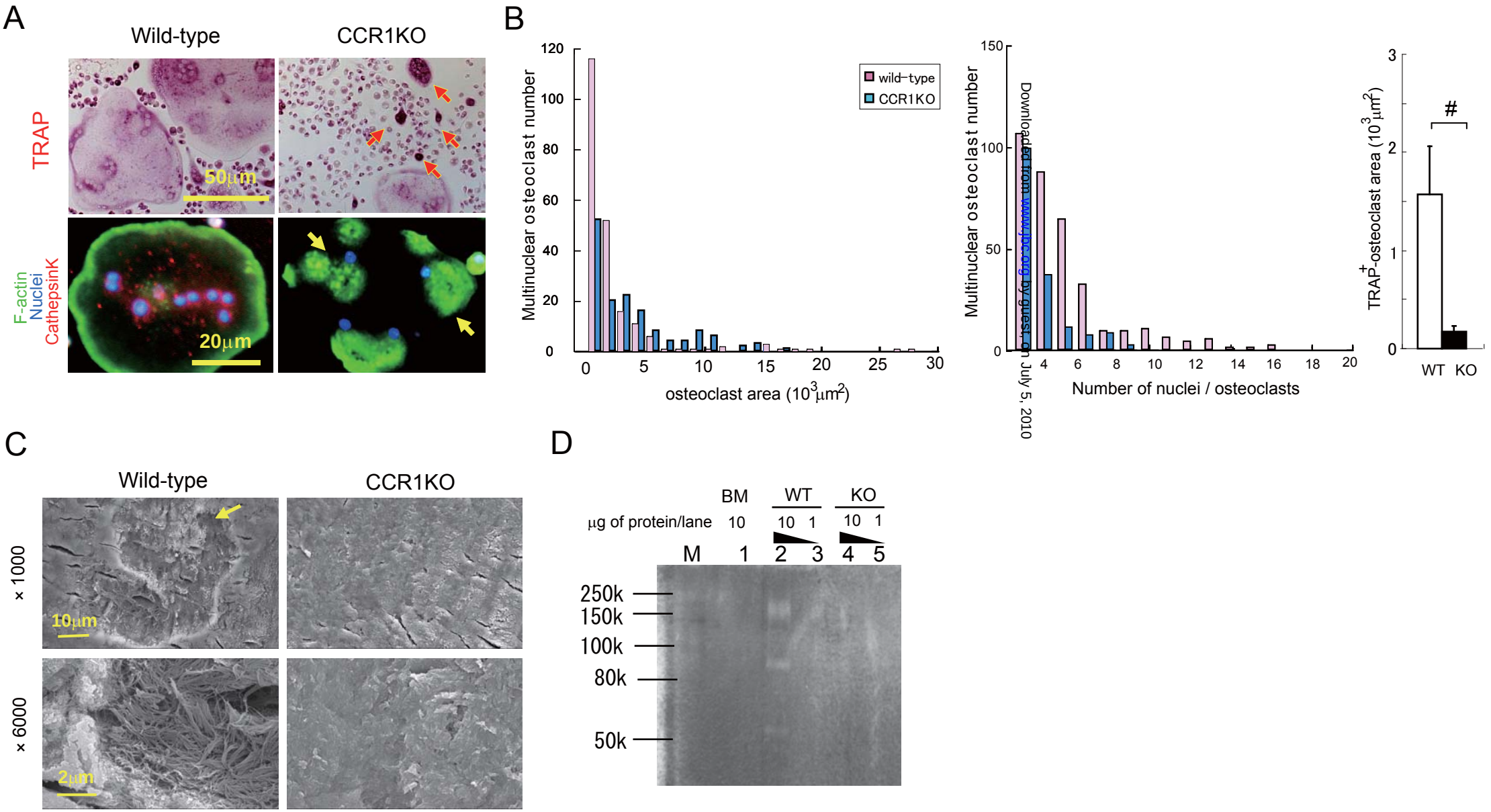

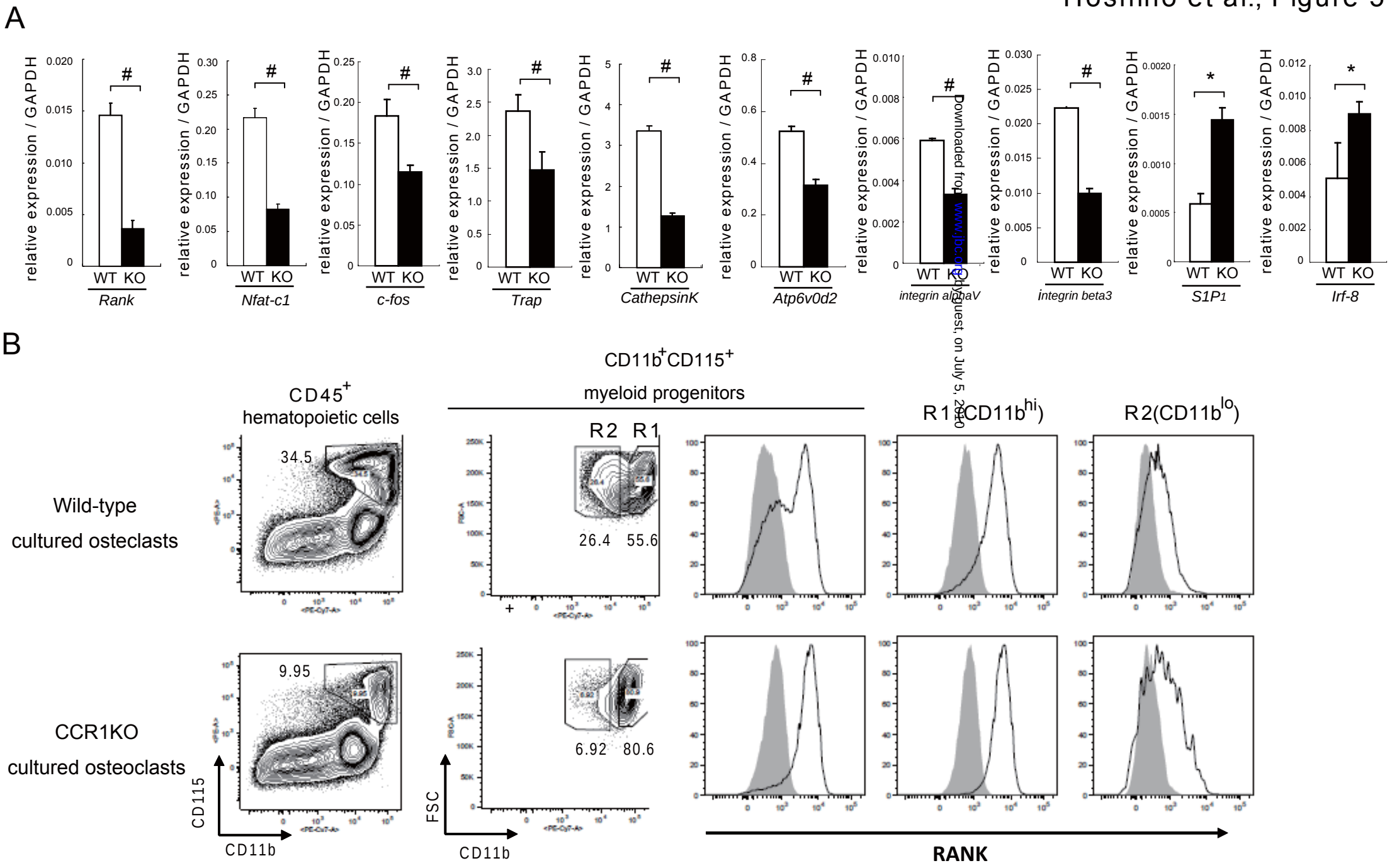

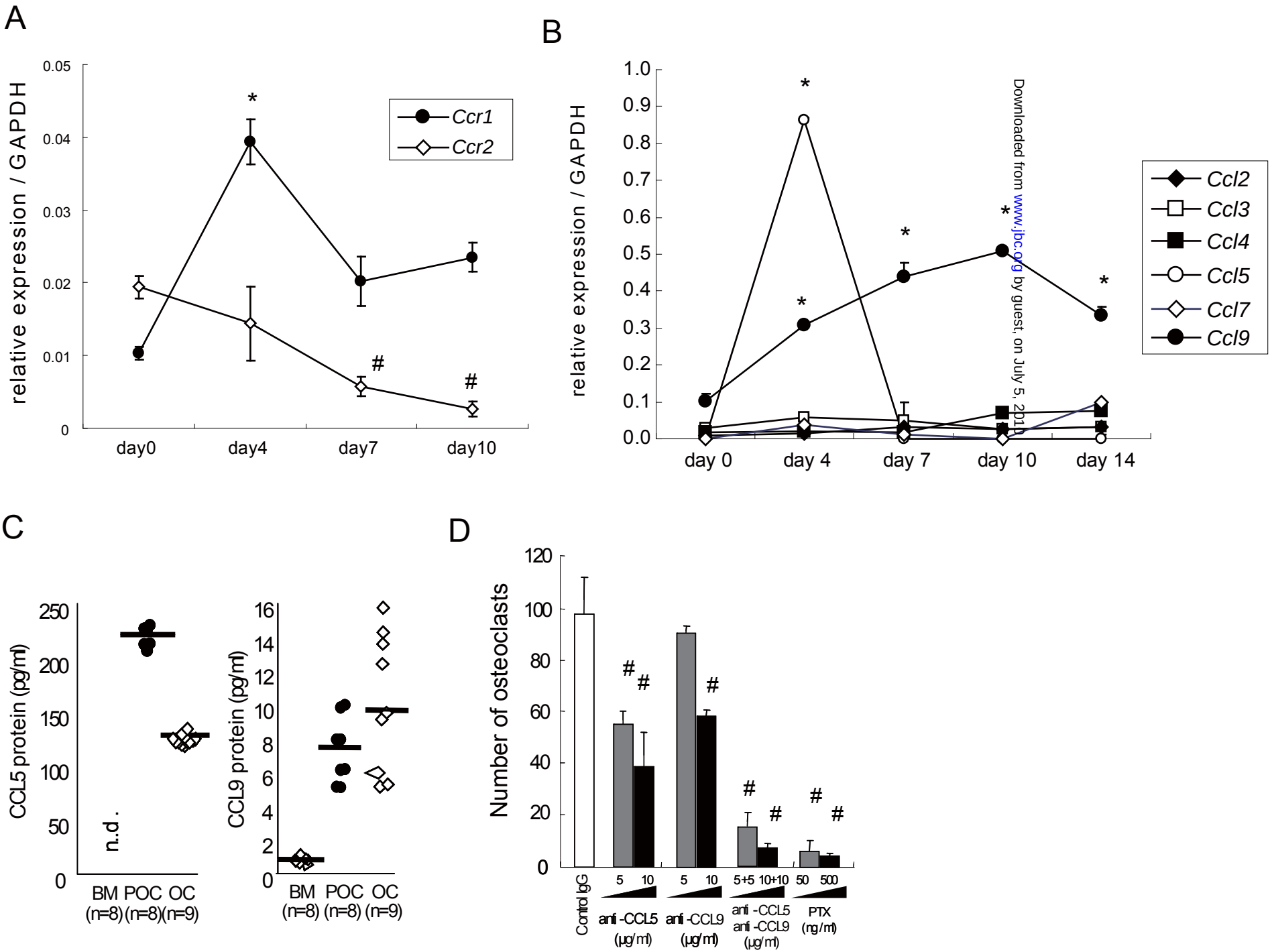
A
relative expression / GAPDH
0.05
0.04
0.03
0.02
0.01
0
day0
day4
day7
day10
Ccr1
Ccr2
*
#
#
B
relative expression / GAPDH
1.0
0.9
0.8
0.7
0.6
0.5
0.4
0.3
0.2
0.1
0.0
day 0
day 4
day 7
day 10
day 14
Ccl2
Ccl3
Ccl4
Ccl5
Ccl7
Ccl9
Downloaded from www.jbc.org by guest, on July 5, 2019
C
CCL5 protein (pg/ml)
250
200
150
100
50
0
n.d.
BM POC OC
(n=8) (n=8) (n=9)
CCL9 protein (pg/ml)
16
14
12
10
8
6
4
2
0
BM POC OC
(n=8) (n=8) (n=9)
D
Number of osteoclasts
120
100
80
60
40
20
0
Control IgG
5 10
anti -CCL5 (μg/ml)
5 10
anti -CCL9 (μg/ml)
5+5 10+10
anti -CCL5 anti -CCL9 (μg/ml)
50 500
PTX (ng/ml)
#